https://doi.org/10.52131/jmps.2020.0102.0008

Journal of Materials and Physical Sciences

Volume 1, Number 2, 2020, Pages 78 - 86

Journal Homepage:
https://journals.internationalrasd.org/index.php/jmps

Comparison of Thermoelectric Properties of ZnO and ZnSnO Thin Films Grown on Si Substrate by Thermal Evaporation

U. Rehman[1], K. Mahmood[1*], A. Ali[1], S. Ikram[1]

[1] Department of Physics, Government College University Faisalabad

ARTICLE INFO

Article History:
Received: October 13, 2020
Revised: November 08, 2020
Accepted: December 06, 2020
Available Online: December 31, 2020

Keywords:
ZnO
ZTO
Seebeck Coefficient
Power Factor
Post Growth Annealing

ABSTRACT

In this manuscript, we compared the thermoelectric properties of ZnO and ZnSnO thin films grown on silicon (100) substrate. We have evaporated Zn and Sn+Zn metal powders were evaporated in vacuum tube furnace alternatively, under same experimental conditions for the growth of ZnO and ZTO respectively. After the deposition, these grown films were cut into pieces and post growth annealed at different annealing temperatures from 600°C to 800°C in the air using programmable muffle furnace. Seebeck and Hall data suggested that ZTO sample shows highest value of Seebeck coefficient, electrical conductivity and power factor as compared to the ZnO samples. It is also observed that the value of Seebeck coefficient showing an increasing trend for both of the samples as we increase the post growth annealing temperature. The higher thermoelectric properties for ZTO are due the presence of Sn atoms in ZnO structure. Tin dopants may generate secondary phases and/or enhanced the carrier mobility which might be the reason that ZTO has improved thermo-electric properties as compared to ZnO. XRD and Raman measurements were used to confirm the formation of ZTO. XRD data verified the hexagonal structure of ZnO but a slight red shift is observed for the case of ZTO samples. To further justify our argument, we have also performed Raman spectroscopy measurements which confirmed the presence of Sn elements in ZTO.

*Corresponding Author's Email: Khalid_mahmood856@yahoo.com

1. Introduction

High temperature thermoelectric materials are getting much interest, especially for the utilization of waste heat from thermal power plants, factories and radioisotope thermoelectric materials for space applications (Kristiansen, Barragán, & Kjelstrup, 2019; Mirhosseini, Rezania, & Rosendahl, 2019; Yuan et al., 2019). However, the real-time applications of many of the thermoelectric materials are limited because of their phase transition at elevated temperatures (Ng et al., 2019). Oxide based thermoelectric materials are getting much interest because they are chemically stable at high temperature (Manickam & Biswas, 2019). ZnO with a wide band gap (3.3 eV) and n-type conductivity is widely used in many electronic applications such as: optical devices, piezoelectric devices, transparent electrode layer for solar applications, integrated circuits and gas sensors (Abed, Ali, Addad, & Elhouichet, 2019; Arrabito, Errico, Zhang, Han, & Falconi, 2018; Kumar, Jeong, & Lee, 2019; Novak et al., 2019; R et al., 2018). Beside this, such a wide band gap of ZnO is beneficial for preventing thermal excitation of the carriers.

Due to its unique properties, ZnO is getting popular for thermoelectric applications, but lower electrical conductivity value limited its applications (Zahra, Mahmood, et al.,

2019). The incorporation of some impurity atom is an easy way to engineer the properties of any material. In addition, insertion of several kinds of donor impurities has been reported so far such as: Al, Ga, Cu, Ni, Ge, In, Sn, Mn and many others to improve the thermoelectric properties of ZnO (Aboud, Shaban, & Revaprasadu, 2019; Ardyanian, Moeini, & Azimi Juybari, 2014; Jayathilake, Sagu, & Wijayantha, 2019; Paul, Khranovskyy, Yakimova, & Eklund, 2019; Teehan, Efstathiadis, & Haldar, 2011; Zahra, Jacob, et al., 2019). The performance of thermoelectric material can be expressed by Seebeck coefficient $(S = \Delta V / \Delta T)$, power factor ($P = S^2 * \sigma$) and dimensionless figure of merit (ZT) which is given by $(ZT = S^2 \sigma T / \mathrm{K})$ (Ali et al., 2019; Ashfaq et al., 2019; Jacob et al., 2019; Mahmood, Abbasi, Zahra, & Rehman, 2018). Where S, σ and K are Seebeck coefficient, electrical conductivity and thermal conductivity respectively.

Tin is supposed to be a donor impurity to improve the electrical and thermoelectric performance of ZnO (Zhang et al., 2019). In addition, both Zn and Sn have almost equal atomic radii make it easy to replace Zn with Sn atom without any degradation in crystal quality. Ajili et al. studied the doping effect of Sn on ZnO and found that 0.6% Sn doping significantly enhance the hall mobility 9.22 cm^2/Vs and resistivity value upto $8.32\times10^{-2}\Omega cm$ (Ajili, Castagné, & Turki, 2013). Recently, Rehman et al. has reported the direct growth of ZnSnO (ZTO) nanowire by thermal evaporation and found that the value of Seebeck coefficient and electrical conductivity was increasing from 220 to 498 μV/°C and 89 to 283 (S/cm) by increasing the post annealing temperature (Rehman et al., 2019).

In this research work, we make a comparison of the thermoelectric properties of ZnO an ZTO thin films grown on silicon substrates by thermal evaporation technique and studied the effect of incorporation of Sn and post growth annealing effect on ZnO. XRD measurements were performed to understand the structural properties which confirm the formation of hexagonal structure. While the Seebeck coefficient and electrical conductivity are found to be increasing with the addition of Sn and post growth annealing temperature.

2. Experimental Detail

In this research work ZnO and ZTO thin films were deposited by thermal evaporation technique by using horizontal glass tube furnace. Initially for ZnO film, 99% pure Zinc powder (0.1g) and for ZTO; Zinc and tin metal powder (10:1) were evaporated on the single crystal Silicon substrate. The detail of experimental work is reported elsewhere (Rehman et al., 2019). After the deposition, samples were cut into rectangular pieces and post growth annealed at different annealing temperatures from 600°C to 800°C at atmospheric pressure in programmable muffle furnace. Finally, samples were characterized by different tools. Structural characterization of the grown thin film was performed by X-ray diffraction (Bruker D8 Advanced) with CuKα source having wavelength 0.154nm. Raman spectroscopy was carried out using MN STEX-PR1100 to study the vibrational and rotational modes of the grown film. The surface morphology of the prepared samples was characterized by EMCRAFT scanning electron microscope (Cube-Series). The Seebeck coefficient was measured by the homemade Seebeck system. The thickness of as grown sample was calculated by thickness meter (Filmtronics) and it was found to be 0.5μm. The detail of the equipment with model number and specifications were already reported in our previous work (Ali et al., 2019).

3. Result and Discussion

Figure 1 (a, b) depicts the effect of post growth annealing and measurement temperature on the Seebeck coefficientof ZnO and ZTO thin films grown on Silicon (100) substrate. The values of Seebeck coefficient for all samples have negative values, showing the n-type behavior for both thin films. The data evident that the value of Seebeck coefficient has shown an increasing trend with annealing temperature for both samples. This behavior of Seebeck coefficient is due to the fact that oxygen atoms diffused to interstitial sites by getting thermal energy due to high annealing temperature which resulted in the increase of Seebeck coefficient. It is accepted fact that annealing temperature filled the oxygen vacancies for example reported by Asghar et al (Asghar, Mahmood, & Hasan, 2012). Even further annealing causes diffusion of oxygen atoms to

interstitials sites. Therefore, for the verification of oxygen vacancies we have performed PL measurements on representative sample shown in figure 2. The graph showed a defect emission peaks. It is believed that defect emission at 2.3 eV is related to the transition from oxygen vacancy to valance band. The graph showed that defect emission decreases as the annealing temperature increases from 600 to 800 ^{0}C because number of oxygen vacancies were filled by incoming oxygen atoms during annealing process. Here we claimed that the addition of donor impurity increases the value of Seebeck coefficient in ZnO metrics. On the other hand, high temperature annealing also causes intrinsic impurity defects and shift scattering mechanism from lattice to impurity scattering mechanism. Hence, carriers are more mobile at high measurement temperature and easily move from hot to cold end so this kind of enhancement in Seebeck coefficient is expected. In recent the same kind of behavior was already reported by our group (Jacob et al., 2019).

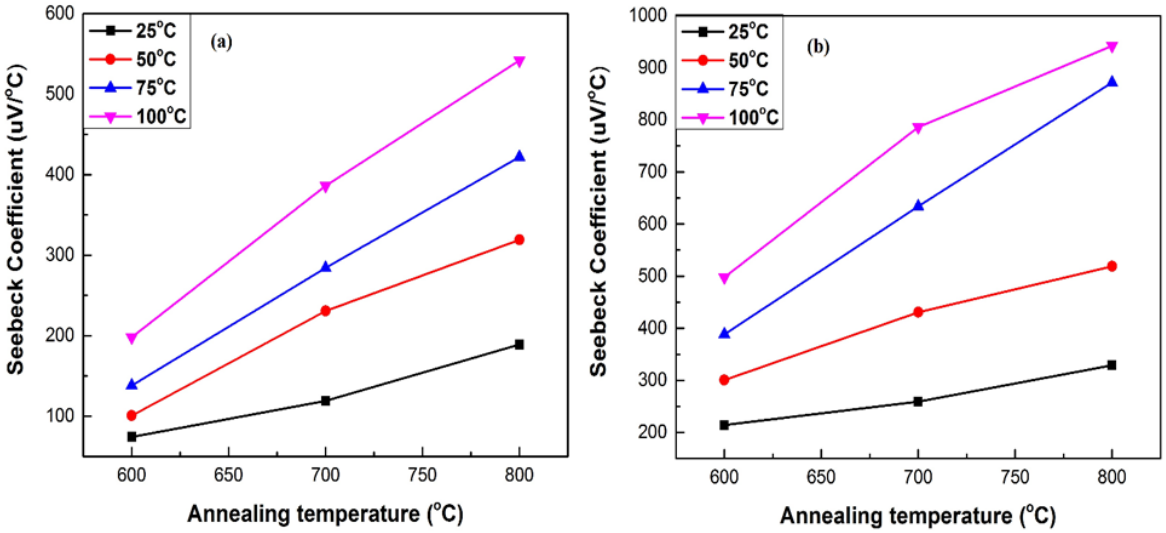

Figure 1: Seebeck coefficient of post annealed(a) ZnO and(b) ZTO thin films at different temperatures ranges from 600-800°C for 60 min at different measurement temperature

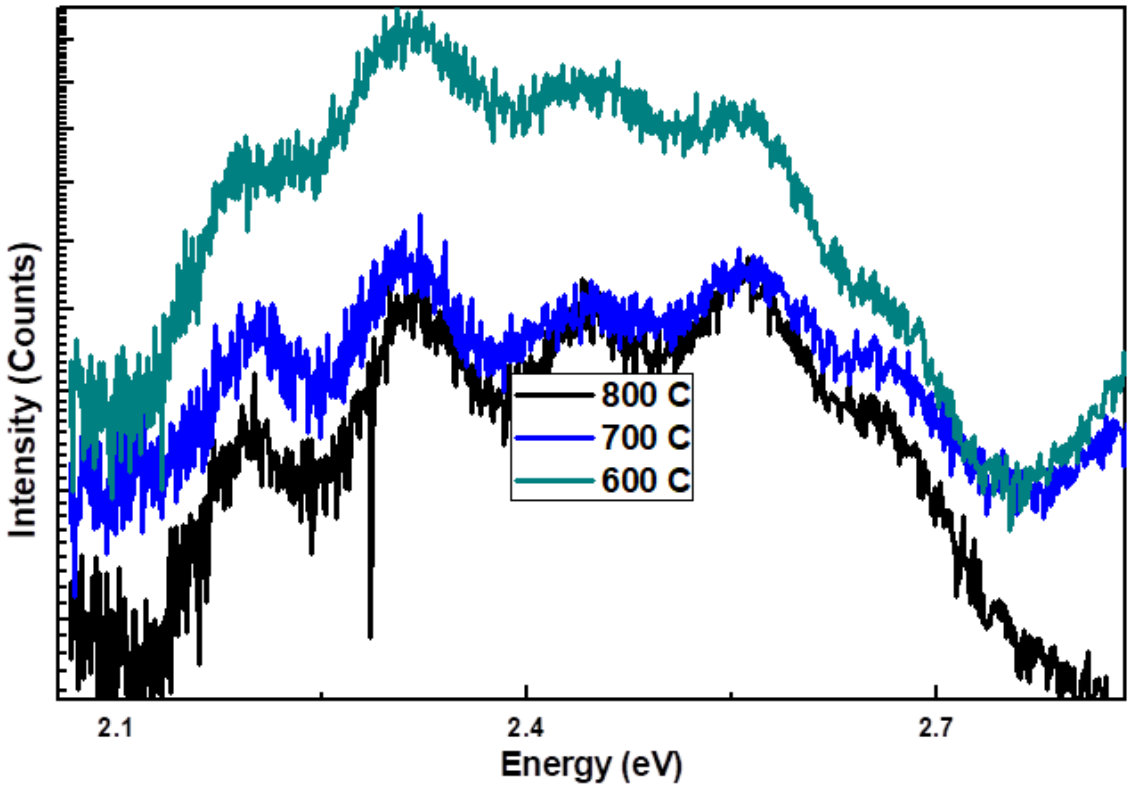

Figure 2: Room temperature PL spectra of ZnO thin films annealed at various temperatures

Figure 3 (a, b) represents the effect of annealing temperature on electrical conductivity of the ZnO and ZTO thin films grown on Si substrate. It is clearly seen that electrical conductivity shows an increasing trend with the annealing temperature. Furthermore, ZTO samples show slightly higher electrical conductivity as compared to ZnO. It can be explained as; ZnO exhibits high electrical conductivity due to the presence of oxygen vacancies acting like a donor state, while the addition of donor impurity can further assist to improve the electrical conductivity. Here in this case addition of Sn^{4+} atom behaves as a doubly ionized donor state so this increase in electrical conductivity is expected (Ruzgar & Caglar, 2019).

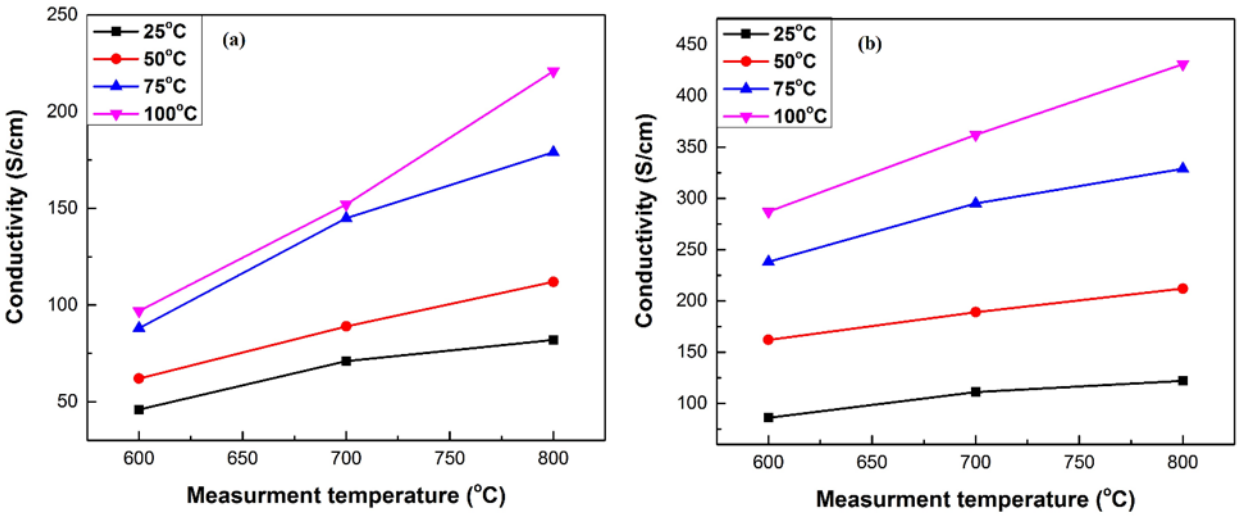

Figure 3: Electrical conductivity of post annealed(a) ZnO and (b) ZTO thin films at different temperatures ranges from 600-800°C for 60 min at different measurement temperature

The effect of annealing temperature on power factor of ZnO and ZTO samples annealed at different annealing temperature is shown in figure 4 (a, b). As electrical conductivity and Seebeck coefficient increased with annealing temperature so increase in power factor for both samples is understandable. As the XRD and Raman data (explained later) have confirmed the presence of Sn atoms into the ZnO sample. These Sn atoms act like donor defects in the ZnO crystal, therefore enhanced the carrier concentration. This enhancement in carrier concentration resulted in the enhancement of Seebeck coefficient and power factor.

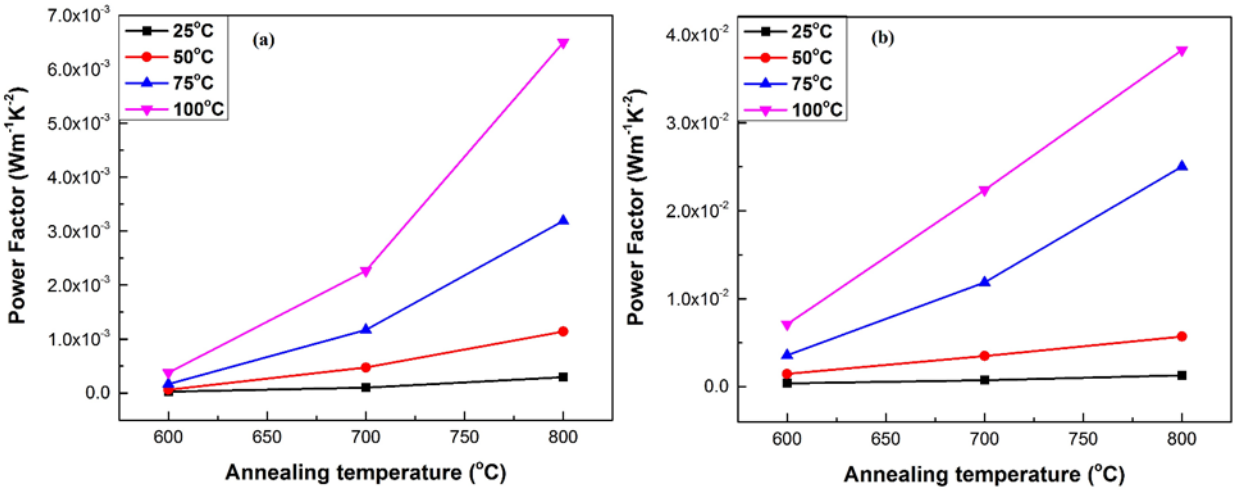

Figure 4: Power factor of post annealed (a) ZnO and (b) ZTO thin films at different temperatures ranges from 600-800°C for 60 min at different measurement temperature

Figure 5 (a, b) demonstrated the XRD pattern of ZnO and ZTO samples at different post growth annealing temperatures. The XRD pattern of post growth annealed samples shows five diffraction peaks. The peak at 31.94°, 34.63°, 36.41°, 47.71° and 56.86° are

related to (100), (002), (101), (102) & (110) which are belongs to wurtzite hexagonal ZnO phase (Ullah, Amin Badshah, Raza, Altaf, & Hussain, 2011). While in the case of ZTO, the diffraction pattern shows the same trend as that of ZnO. No other secondary phases related to SnO and SnO_2 are observed with the addition of the impurity atoms in ZnO crystal. Only a slight shift toward the higher angle is observed for ZTO sample as compare to the pure ZnO sample. This behavior is attributed as: when larger radii atom (Zn=74 pm) is replaced with the smaller radii atom (Sn=70 pm) this red shift is expected (Ajili et al., 2013). To strengthen our argument and to verify the presence of Sn, we perform Raman spectroscopy measurements (latterly discussed). In fig. 4 (a) the plane along (101) shows the maximum intensity for ZnO while in case of ZTO the preferred peak along (002) is observed fig. 5 (b). This means these planes are sensitive to the oxygen which is already reported in literature (Chahmat et al., 2014). It is clearly seen that crystallinity of the film is decreased as the post growth annealing temperature is increased. This could be explained as more and more oxygen atoms trying to occupy the interstitial sites causing degradation in crystallinity of the film.

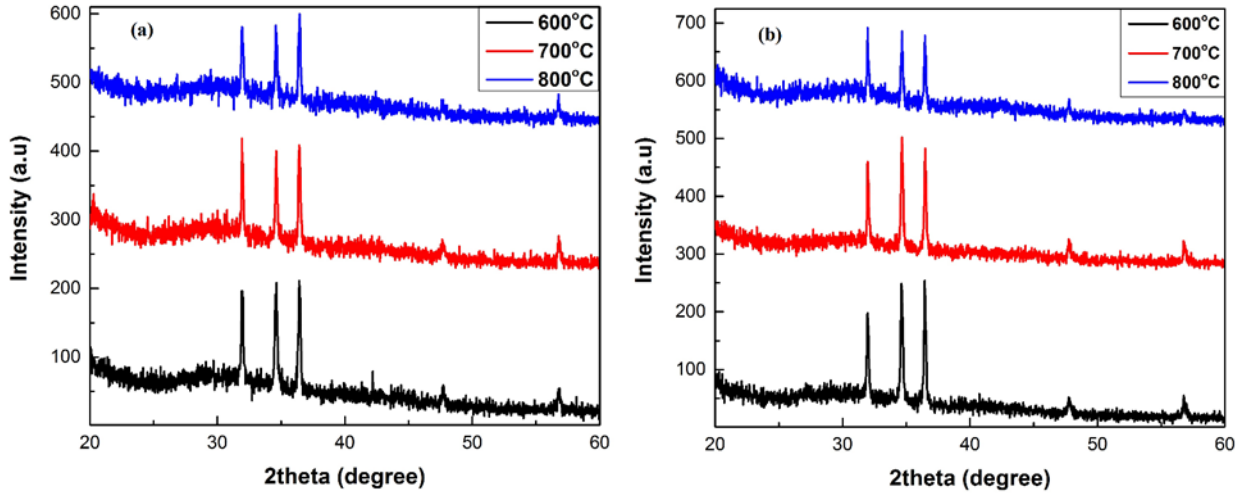

Figure 5: XRD pattern of post annealed (a) ZnO and (b) ZTO thin films at different temperatures ranges from 600-800°C for 60 min.

Figure 6 (a, b) shows the Raman spectra of ZnO and ZTO thin films to understand the behavior of vibrational and rotational modes by varying the post growth annealing temperature from 600°C to 800°C. For both spectrums two major peaks at 437 cm^{-1} and 521cm^{-1} are present, which are related to the E_g mode of ZnO and translational optical phonon mode of single crystal silicon respectively (Montenegro et al., 2013; Sahu, 2013). We have also observed a small peak at 302cm^{-1} related to double acoustic phonon mode of Si and a peak at 458cm^{-1} is related to δ mode Si-O (Ferreira, Santos, Bonacin, Passos, & Pocrifka, 2015; Tyschenko, Volodin, & Popov, 2019).The peaks appear at 379 cm^{-1} and574 cm^{-1} are assigned as A_1(TO),A_1(LO) modes while the peaks at 410 cm^{-1},and 585 $cm^{-1}$are related to E1 (TO) and E_1 (LO) modes of pure ZnO (Cuscó et al., 2007). On the other hand, a large hump around 328$cm^{-1}$is related to $E_2^{high} - E_2^{low}$ non-polar modes of ZnO. The presence of $E_2^{high} - E_2^{low}$ mode is occurred due to vibration of Zinc sublattice and the motion of oxygen atoms (Horzum et al., 2019). Furthermore, a very small distortion at 614cm^{-1} is present, which is attributed to combined optical and acoustic mode of ZnO. But in case of ZTO samples fig. 6 (b) the peaks around 235 cm^{-1}, 478 cm^{-1} and 546 cm^{-1} appears, which can be assigned to E_u (1)TO,E_g and A_{2u} TO mode of SnO_2while the peak at 662 cm^{-1} is related to asymmetric vibration of Sn-O-Sn (Mereu, Le Donne, Trabattoni, Acciarri, & Binetti, 2015). The presence of Sn elements in Raman spectra further clarified our argument of the formation of ZTO.

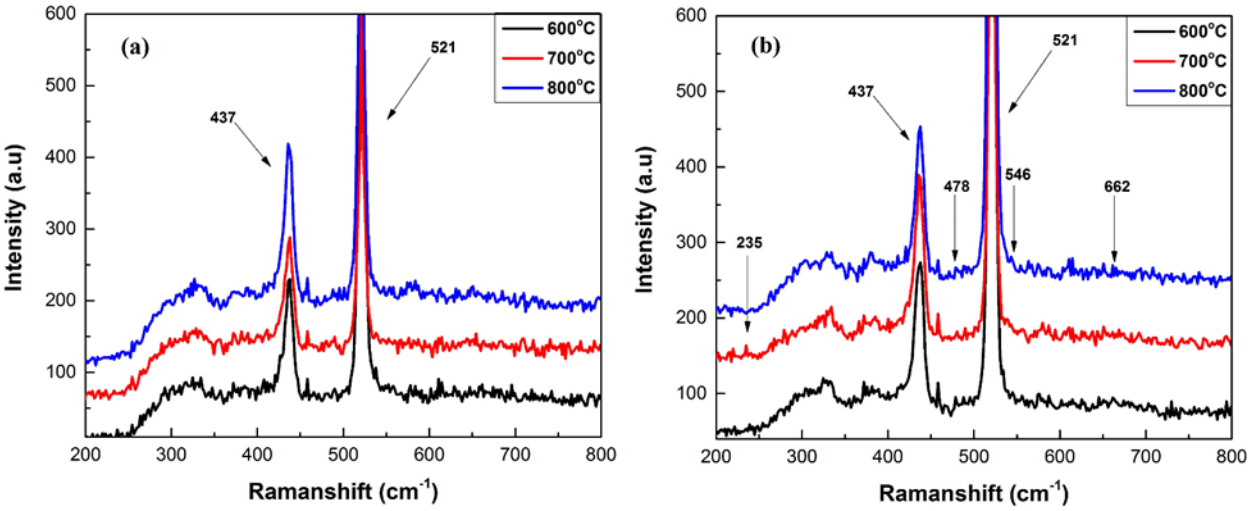

Figure 6: Raman spectrum of post annealed (a) ZnO and (b) ZTO thin films at different temperatures ranges from 600-800°C for 60 min.

Figure 7 depicts the SEM images of as grown and annealed ZTO samples grown by thermal evaporation. SEM image of as grown sample demonstrated the nano-structure morphology of sample but such nanostructures were disappeared when sample annealed at different temperatures. The disappearance of such structures is due to the incorporation of metallic ions into the grown films due to oxidation.

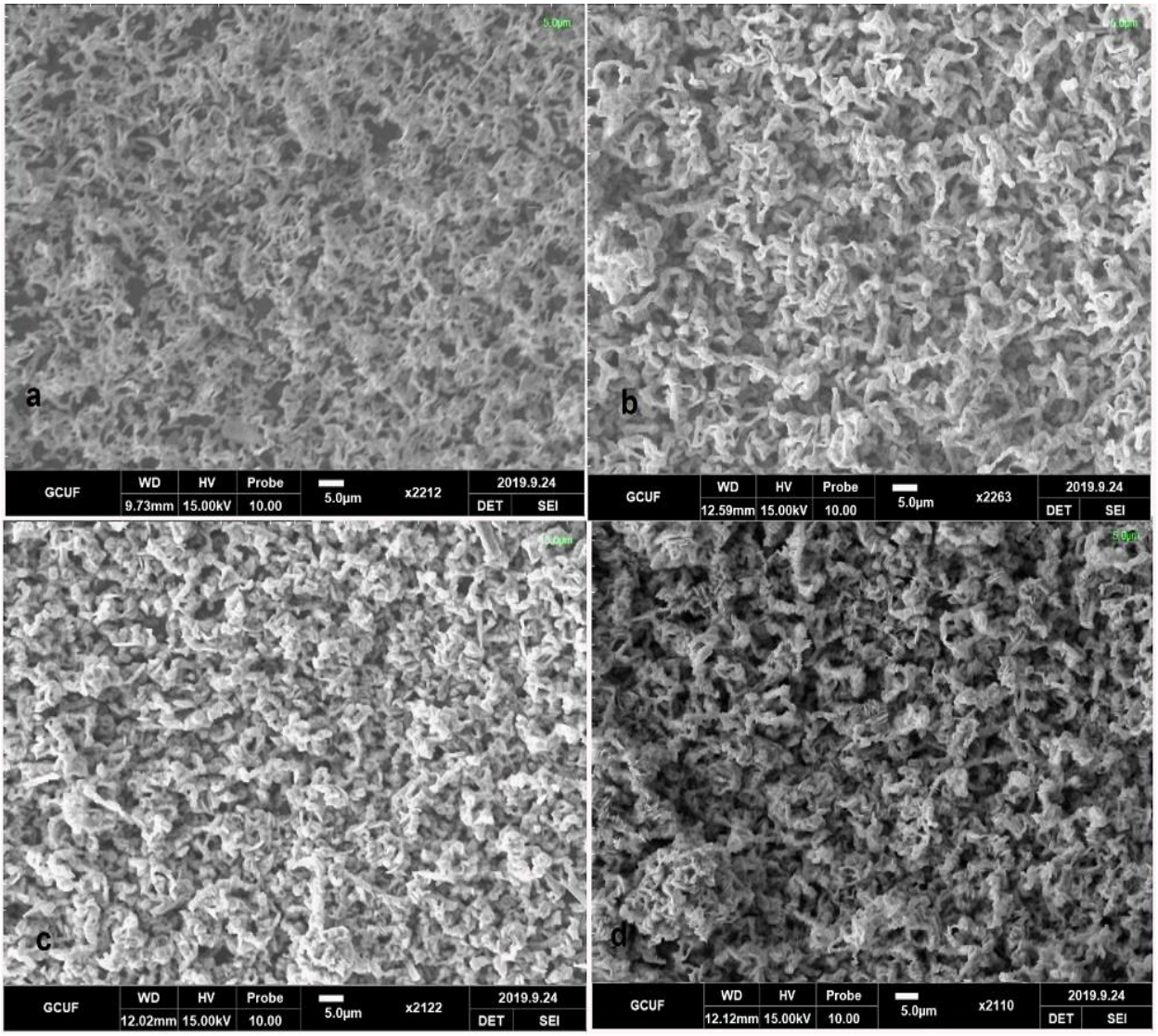

Figure 7: (a) (b) (c) (d) SEM images of as grown and annealed ZTO samples

4. Conclusion

In this research work, we have compared the post growth annealing effect on the thermoelectric properties of ZnO and ZTO thin films grown on Si substrate and explore its potential for thermoelectric power generation applications. XRD data confirm the formation of hexagonal structure for both samples while the Raman spectroscopy measurements verified the presence of Sn elements in the ZTO samples. The temperature dependent Seebeck and Hall measurements were performed to understand the behavior of Seebeck coefficient with post growth annealing and measurement temperature. It is found that the ZTO sample shows better thermoelectric properties as compared to ZnO sample.

References

Abed, C., Ali, M. B., Addad, A., & Elhouichet, H. (2019). Growth, structural and optical properties of ZnO-ZnMgO-MgO nanocomposites and their photocatalytic activity under sunlight irradiation. *Materials Research Bulletin, 110*, 230-238. doi:https://doi.org/10.1016/j.materresbull.2018.10.041

Aboud, A. A., Shaban, M., & Revaprasadu, N. (2019). Effect of Cu, Ni and Pb doping on the photo-electrochemical activity of ZnO thin films. *RSC advances, 9*(14), 7729-7736. doi:10.1039/C8RA10599E

Ajili, M., Castagné, M., & Turki, N. K. (2013). Study on the doping effect of Sn-doped ZnO thin films. *Superlattices and Microstructures, 53*, 213-222. doi:https://doi.org/10.1016/j.spmi.2012.10.012

Ali, A., Jacob, J., Ashfaq, A., Tamseel, M., Mahmood, K., Amin, N., . . . Al-Othmany, D. S. (2019). Modulation of structural, optical and thermoelectric properties of sol-gel grown CZTS thin films by controlling the concentration of zinc. *Ceramics International, 45*(10), 12820-12824. doi:https://doi.org/10.1016/j.ceramint.2019.03.202

Ardyanian, M., Moeini, M., & Azimi Juybari, H. (2014). Thermoelectric and photoconductivity properties of zinc oxide–tin oxide binary systems prepared by spray pyrolysis. *Thin Solid Films, 552*, 39-45. doi:https://doi.org/10.1016/j.tsf.2013.12.010

Arrabito, G., Errico, V., Zhang, Z., Han, W., & Falconi, C. (2018). Nanotransducers on printed circuit boards by rational design of high-density, long, thin and untapered ZnO nanowires. *Nano Energy, 46*, 54-62. doi:https://doi.org/10.1016/j.nanoen.2018.01.029

Asghar, M., Mahmood, K., & Hasan, M. A. (2012). Investigation of Source of N-Type Conductivity in Bulk ZnO. *Key Engineering Materials, 510-511*, 227-232. doi:10.4028/www.scientific.net/KEM.510-511.227

Ashfaq, A., Jacob, J., Bano, N., Ali, A., Ahmad, W., Mahmood, K., . . . Hussain, S. (2019). Tailoring the thermoelectric properties of sol-gel grown CZTS/ITO thin films by controlling the secondary phases. *Physica B: Condensed Matter, 558*, 86-90. doi:https://doi.org/10.1016/j.physb.2019.01.043

Chahmat, N., Souier, T., Mokri, A., Bououdina, M., Aida, M. S., & Ghers, M. (2014). Structure, microstructure and optical properties of Sn-doped ZnO thin films. *Journal of Alloys and Compounds, 593*, 148-153. doi:https://doi.org/10.1016/j.jallcom.2014.01.024

Cuscó, R., Alarcón-Lladó, E., Ibáñez, J., Artús, L., Jiménez, J., Wang, B., & Callahan, M. J. (2007). Temperature dependence of Raman scattering in ZnO. *Physical Review B, 75*(16), 165202. doi:10.1103/PhysRevB.75.165202

Ferreira, C. S., Santos, P. L., Bonacin, J. A., Passos, R. R., & Pocrifka, L. A. (2015). Rice Husk Reuse in the Preparation of SnO2/SiO2Nanocomposite. *Materials Research, 18*, 639-643. doi:https://doi.org/10.1590/1516-1439.009015

Horzum, S., Iyikanat, F., Senger, R. T., Çelebi, C., Sbeta, M., Yildiz, A., & Serin, T. (2019). Monitoring the characteristic properties of Ga-doped ZnO by Raman spectroscopy and atomic scale calculations. *Journal of Molecular Structure, 1180*, 505-511. doi:https://doi.org/10.1016/j.molstruc.2018.11.064

Jacob, J., Wahid, R., Ali, A., Zahra, R., Ikram, S., Amin, N., . . . Mahmood, K. (2019). Growth of Cu2InO4 thin films on Si substrate by thermal evaporation technique and enhancement of thermoelectric properties by post-growth annealing. *Physica B: Condensed Matter, 562*, 59-62. doi:https://doi.org/10.1016/j.physb.2019.03.023

Jayathilake, D. S. Y., Sagu, J. S., & Wijayantha, K. G. U. (2019). Transparent heater based on Al,Ga co-doped ZnO thin films. *Materials Letters, 237*, 249-252. doi:https://doi.org/10.1016/j.matlet.2018.11.092

Kristiansen, K. R., Barragán, V. M., & Kjelstrup, S. (2019). Thermoelectric Power of Ion Exchange Membrane Cells Relevant to Reverse Electrodialysis Plants. *Physical Review Applied, 11*(4), 044037. doi:10.1103/PhysRevApplied.11.044037

Kumar, M., Jeong, H., & Lee, D. (2019). UV photodetector with ZnO nanoflowers as an active layer and a network of Ag nanowires as transparent electrodes. *Superlattices and Microstructures, 126*, 132-138. doi:https://doi.org/10.1016/j.spmi.2018.12.004

Mahmood, K., Abbasi, S., Zahra, R., & Rehman, U. (2018). Investigation of large Seebeck effect by charge mobility engineering in CuAlO2 thin films grown on Si substrate by thermal evaporation. *Ceramics International, 44*(15), 17905-17908. doi:https://doi.org/10.1016/j.ceramint.2018.06.263

Manickam, R., & Biswas, K. (2019). Double doping induced power factor enhancement in CuCrO2 for high temperature thermoelectric application. *Journal of Alloys and Compounds, 775*, 1052-1056. doi:https://doi.org/10.1016/j.jallcom.2018.10.083

Mereu, R. A., Le Donne, A., Trabattoni, S., Acciarri, M., & Binetti, S. (2015). Comparative study on structural, morphological and optical properties of Zn2SnO4 thin films prepared by r.f. sputtering using Zn and Sn metal targets and ZnO–SnO2 ceramic target. *Journal of Alloys and Compounds, 626*, 112-117. doi:https://doi.org/10.1016/j.jallcom.2014.11.150

Mirhosseini, M., Rezania, A., & Rosendahl, L. (2019). Harvesting waste heat from cement kiln shell by thermoelectric system. *Energy, 168*, 358-369. doi:https://doi.org/10.1016/j.energy.2018.11.109

Montenegro, D. N., Hortelano, V., Martínez, O., Martínez-Tomas, M. C., Sallet, V., Muñoz-Sanjosé, V., & Jiménez, J. (2013). Non-radiative recombination centres in catalyst-free ZnO nanorods grown by atmospheric-metal organic chemical vapour deposition. *Journal of Physics D: Applied Physics, 46*(23), 235302. doi:10.1088/0022-3727/46/23/235302

Ng, H. K., Abutaha, A., Voiry, D., Verzhbitskiy, I., Cai, Y., Zhang, G., . . . Hippalgaonkar, K. (2019). Effects Of Structural Phase Transition On Thermoelectric Performance in Lithium-Intercalated Molybdenum Disulfide (LixMoS2). *ACS Applied Materials & Interfaces, 11*(13), 12184-12189. doi:10.1021/acsami.8b22105

Novak, N., Keil, P., Frömling, T., Schader, F. H., Martin, A., Webber, K. G., & Rödel, J. (2019). Influence of metal/semiconductor interface on attainable piezoelectric and energy harvesting properties of ZnO. *Acta Materialia, 162*, 277-283. doi:https://doi.org/10.1016/j.actamat.2018.10.008

Paul, B., Khranovskyy, V., Yakimova, R., & Eklund, P. (2019). Donor-doped ZnO thin films on mica for fully-inorganic flexible thermoelectrics. *Materials Research Letters, 7*(6), 239-243. doi:10.1080/21663831.2019.1594427

R, S. G., M, N., Patil, V. L., S, P., C, M., Kawasaki, S., . . . Hayakawa, Y. (2018). Sensitivity enhancement of ammonia gas sensor based on Ag/ZnO flower and nanoellipsoids at low temperature. *Sensors and Actuators B: Chemical, 255*, 672-683. doi:https://doi.org/10.1016/j.snb.2017.08.015

Rehman, U., Jacob, J., Mahmood, K., Ali, A., Ashfaq, A., Amin, N., . . . Hussain, S. (2019). Direct growth of ZnSnO nano-wires by thermal evaporation technique for thermoelectric applications. *Physica B: Condensed Matter, 570*, 232-235. doi:https://doi.org/10.1016/j.physb.2019.06.042

Ruzgar, S., & Caglar, M. (2019). The effect of Sn on electrical performance of zinc oxide based thin film transistor. *Journal of Materials Science: Materials in Electronics, 30*(1), 485-490. doi:10.1007/s10854-018-0313-5

Sahu, G. (2013). Confinement in MeV Au 2+ implanted Si: a Raman scattering study. *Advances in Natural Sciences: Nanoscience and Nanotechnology, 5*(1), 015002. doi:10.1088/2043-6262/5/1/015002

Teehan, S., Efstathiadis, H., & Haldar, P. (2011). Enhanced power factor of Indium co-doped ZnO:Al thin films deposited by RF sputtering for high temperature thermoelectrics. *Journal of Alloys and Compounds, 509*(3), 1094-1098. doi:https://doi.org/10.1016/j.jallcom.2010.10.004

Tyschenko, I. E., Volodin, V. A., & Popov, V. P. (2019). Raman Scattering in InSb Spherical Nanocrystals Ion-Synthesized in Silicon-Oxide Films. *Semiconductors, 53*(4), 493-498. doi:10.1134/S1063782619040262

Ullah, S., Amin Badshah, F. A., Raza, R., Altaf, A. A., & Hussain, R. (2011). Electrodeposited zinc electrodes for high current Zn/AgO bipolar batteries.

Yuan, Z., Tang, X., Liu, Y., Xu, Z., Liu, K., Li, J., . . . Wang, H. (2019). Improving the performance of a screen-printed micro-radioisotope thermoelectric generator through stacking integration. *Journal of Power Sources, 414*, 509-516. doi:https://doi.org/10.1016/j.jpowsour.2019.01.040

Zahra, R., Jacob, J., Bano, N., Ali, A., Mahmood, K., Ikram, S., . . . Hussain, S. (2019). Effect of secondary phases on the thermoelectric properties of Zn2GeO4 nano-crystals grown by thermal evaporation on Au coated Si substrate. *Physica B: Condensed Matter, 564*, 143-146. doi:https://doi.org/10.1016/j.physb.2019.02.061

Zahra, R., Mahmood, K., Ali, A., Rehman, U., Amin, N., Arshad, M. I., . . . Mahmood, M. H. R. (2019). Growth of Zn2GeO4 thin film by thermal evaporation on ITO substrate for thermoelectric power generation applications. *Ceramics International, 45*(1), 312-316. doi:https://doi.org/10.1016/j.ceramint.2018.09.168

Zhang, Q., Xia, G., Li, L., Xia, W., Gong, H., & Wang, S. (2019). High-performance Zinc-Tin-Oxide thin film transistors based on environment friendly solution process. *Current applied physics, 19*(2), 174-181. doi:https://doi.org/10.1016/j.cap.2018.10.012